Loss of a conserved MAPK causes catastrophic failure in assembly of a specialized cilium-like structure in *Toxoplasma gondii*

William J. O'Shaughnessy[a], Xiaoyu Hu[a], Tsebaot Beraki[a], Matthew McDougal[b], and Michael L. Reese[a,c,*]

[a]Department of Pharmacology, [b]Department of Microbiology, and [c]Department of Biochemistry, UT Southwestern Medical Center, Dallas, TX 75390

ABSTRACT **Primary cilia are important organizing centers that control diverse cellular processes. Apicomplexan parasites like *Toxoplasma gondii* have a specialized cilium-like structure called the conoid that organizes the secretory and invasion machinery critical for the parasites' lifestyle. The proteins that initiate the biogenesis of this structure are largely unknown. We identified the *Toxoplasma* orthologue of the conserved kinase ERK7 as essential to conoid assembly. Parasites in which ERK7 has been depleted lose their conoids late during maturation and are immotile and thus unable to invade new host cells. This is the most severe phenotype to conoid biogenesis yet reported, and is made more striking by the fact that ERK7 is not a conoid protein, as it localizes just basal to the structure. ERK7 has been recently implicated in ciliogenesis in metazoan cells, and our data suggest that this kinase has an ancient and central role in regulating ciliogenesis throughout Eukaryota.**

Monitoring Editor
Fred Chang
University of California, San Francisco

Received: Nov 7, 2019
Revised: Feb 3, 2020
Accepted: Feb 14, 2020

INTRODUCTION

Cilia are specialized organelles that mediate cell motility and signal transduction. In apicomplexan parasites, the cilium was likely adapted to form the organizing core of the "apical complex" of cytoskeletal structures and secretory organelles for which the phylum is named (Figure 1; de Leon *et al.*, 2013). The core of the apical complex is recognizable throughout Apicomplexa (Hepler *et al.*, 1966; Aikawa, 1967; Lumb *et al.*, 1988) and may have evolved much earlier, as analogous structures are found in related free-living Alveolates (Okamoto and Keeling, 2014; Portman *et al.*, 2014). The protein components of the apical complex include orthologues of cilium-associated proteins including centrins (Hu *et al.*, 2006; Lentini *et al.*, 2019), a SAS6 cartwheel protein (de Leon *et al.*, 2013; Lévêque *et al.*, 2016), an associated rootlet fiber (Francia *et al.*, 2012), and a distributed microtubule-organizing center called the apical polar ring (Leung *et al.*, 2017). During the asexual stage, most Apicomplexa, including *Toxoplasma*, have a specialized cilium-like structure called the conoid, and typical motile flagella grow at this site during the sexual stage (Francia *et al.*, 2015). As in ciliogenesis in model organisms, the *Toxoplasma* apical complex splits from the centrosome early during daughter cell budding (Anderson-White *et al.*, 2012), but the molecular mechanisms that regulate this biogenesis are unknown.

Here, we describe the essential role of the *Toxoplasma* orthologue of ERK7 in apical complex biogenesis. We found that ERK7 localizes to the apical end of the parasite throughout the cell cycle, suggesting a role in the parasite invasion machinery. Consistent with this hypothesis, we found that parasites lacking ERK7 protein have a complete block in egress and invasion. Without ERK7, parasites fail to develop a conoid, suggesting that ERK7 is required for its biogenesis. Even though ERK7 does not appear to be conoid-localized, its depletion causes complete loss of the conoid in mature parasites. ERK7 is an understudied mitogen-activated protein kinase (MAPK)

This article was published online ahead of print in MBoC in Press (http://www.molbiolcell.org/cgi/doi/10.1091/mbc.E19-11-0607) on February 19, 2020.

*Address correspondence to: Michael L. Reese (Michael.Reese@UTSouthwestern.edu).

Abbreviations used: AID, auxin-inducible degron; Cb, chromobody; DMEM, Dulbecco's Modified Eagle Medium; eGFP, enhanced green fluorescent protein; ERK, extracellular signal-regulated kinase; GFP, green fluorescent protein; HFF, human foreskin fibroblasts; HRP, horse radish peroxidase; IAA, indole-3-acetic acid; ISP1, IMC sub-compartment protein 1; MAPK, mitogen-activated protein kinase; MIC, micronemal protein; PLP1, perforin like protein 1; PV, parasitophorous vacuole; RNG1, ring-1; RON11, rhoptry neck protein 11; ROP2, rhoptry protein 2; SAS6L, spindle assembly abnormal protein 6-like; SIM, structured illumination microscopy; SP, signal peptide; TEM, transmission electron microscopy; TIR1, transport inhibitor response protein 1; 3xHA, 3x Hemagglutinin Tag.

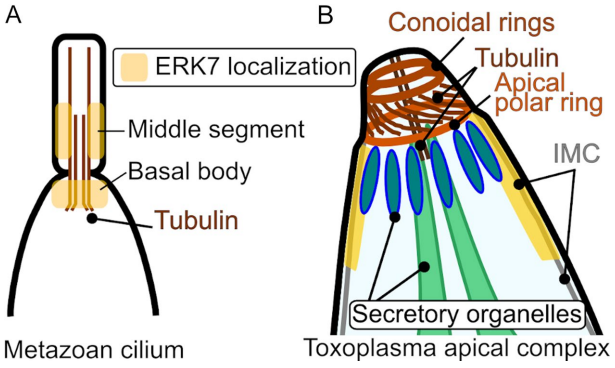

FIGURE 1: A cartoon comparing the (A) metazoa cilium and (B) *Toxoplasma* apical complex.

that is conserved throughout Eukaryota. Our findings are consistent with recent reports implicating metazoan ERK7 in ciliogenesis in invertebrate and vertebrate models (Miyatake *et al.*, 2015; Kazatskaya *et al.*, 2017), and suggest that the MAPK ERK7 is an essential component of the core machinery that regulates ciliogenesis throughout Eukaryota.

RESULTS AND DISCUSSION

ERK7 is a conserved MAPK localized at the apical end of the parasite

The *Toxoplasma* genome encodes three predicted MAPKs. To assess whether the *Toxoplasma* gene TGME49_233010 is, indeed, a member of the ERK7 family, we estimated the phylogenetic tree from an alignment of ERK7 sequences from diverse organisms (Supplemental Figure S1), including other members of the CMGC kinase family as outgroups. The phylogenetic tree shows high bootstrap support for the TGME49_233010 as a member of this family.

To determine ERK7 localization within the parasite, we used CRISPR-mediated homologous repair to tag the endogenous locus with a C-terminal 3xHA epitope tag. Immunofluorescence analysis shows ERK7 signal concentrates at the apical end of the parasite. Specifically, ERK7 colocalizes with the apical cap protein ISP1, just basal to the tubulin-rich parasite conoid (Figure 2A). Furthermore, ERK7 appears to be recruited to this structure early in its biogenesis, as clear foci are evident in both mature parasites and in early daughter buds (Figure 2A). Structured illumination microscopy revealed punctate ERK7 staining throughout the parasites, and confirmed that ERK7 concentrates just basal to the apical complex ring in both mature and daughter parasites. Furthermore, at high resolution, ERK7 does not colocalize with either the parasite cortical microtubules (Figure 2B) or the apical cap cytoskeletal protein ISP1 (Figure 2C).

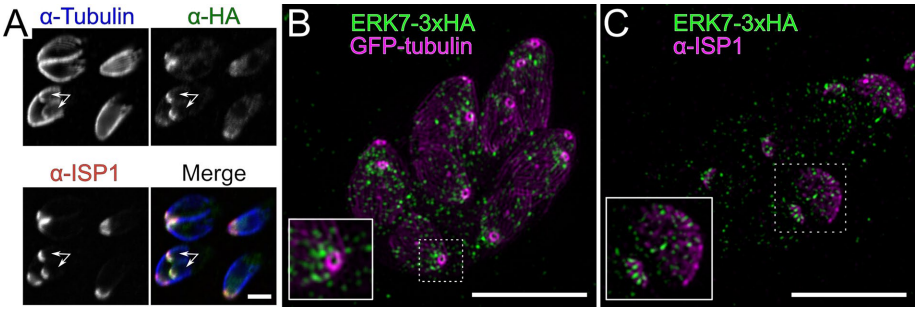

FIGURE 2: ERK7 is apically localized. (A) A 0.5-µm confocal slice of immunofluorescence using antibodies for 3xHA-tagged ERK7 (green), β-tubulin (blue), and the apical cap marker ISP1 (red). Note that anti-tubulin does not stain the conoid, likely due to antigen accessibility. Arrows indicate daughter buds. Scale bar: 3 µm. Maximum intensity projection of SIM stacks of (B) ERK7-3xHA (green) and GFP-α-tubulin (magenta), and (C) ERK7-3xHA (green) and anti-ISP1 (magenta). Scale bars: 5 µm.

ERK7 is essential for parasite invasion and egress

We were unable to obtain ERK7 knockouts using either homologous recombination or CRISPR-mediated strategies. We therefore turned to the auxin-inducible degron (AID) system (Nishimura *et al.*, 2009; Long *et al.*, 2017b), which enables rapid, inducible degradation of a protein. We made a parasite strain in which the ERK7 protein was expressed in frame with an AID and 3xFLAG tag in the background of RH*Δku80* expressing the rice TIR1 auxin response protein (ERK7^{AID}). ERK7 localization was unaffected by the AID tag (Supplemental Figure S2A). We found that ERK7^{AID} protein was rapidly degraded upon addition of the auxin indole-3-acetic acid (IAA), as it was undetectable by Western blot 15 min after IAA treatment (Figure 3A). We will refer to parasites in which ERK7 has been inducibly degraded as ERK7$^{AID/IAA}$. ERK7 was essential for the lytic cycle, as ERK7$^{AID/IAA}$ produced no plaques (Figure 3B). To verify that this phenotype was specific to ERK7 depletion, we made parasites expressing a nondegradable copy of wild-type ERK7-3xHA in the background of the ERK7^{AID} parasites (Supplemental Figure S2, B and C). As expected, wild-type ERK7 rescued the ability of the ERK7$^{AID/IAA}$ parasites to form plaques (Figure 3B). However, we were unable to obtain stable parasites expressing kinase-dead (D136A) ERK7, suggesting expression of kinase-dead protein has a strong fitness cost.

Failure to form plaques can be due to impairments in replication rate, invasion, or egress efficiency. While ERK7 has been suggested to be important for efficient replication (Li *et al.*, 2016), we observed only a modest phenotype in ERK7$^{AID/IAA}$ parasite replication (Figure 3C). This could not explain the lack of plaque formation. Instead, we noted that ERK7$^{AID/IAA}$ parasites replicated until they mechanically disrupted the host cell. After host cell rupture, parasites appeared trapped within their vacuoles, which we found floating in the media (Figure 3D). Such trapped parasites suggest a block in natural egress reminiscent of the deletion of parasite perforin-like protein 1 (PLP1; Kafsack *et al.*, 2009). Parasite egress from host cells can be induced by treatment with the calcium ionophore A23187 (Carruthers and Sibley, 1999). We therefore tested whether ERK7 was essential for induced egress. Parasites were allowed to invade host fibroblasts for 4 h and then grown with or without IAA for 24 h. Egress was induced with ionophore. ERK7$^{AID/IAA}$ parasites showed a complete block in egress (Figure 3E). Notably, when parasites were treated with a brief 1-h exposure to IAA, we observed no phenotype (Figure 3E), indicating that the effects we see require completion of a parasite cell cycle (which takes 6–8 h; Nishi *et al.*, 2008). Consistent with this idea, parasites incubated for 8 h with IAA showed a similar block in egress to those treated for 24 h (Figure 3E).

We next tested whether parasites lacking ERK7 were able to invade host cells. ERK7^{AID} and rescued parasites were grown with or without IAA for 24 h. The parasites were mechanically released from the host cells and an equal number of each strain incubated with fresh host monolayers for 2 h at 37°C. Cells were then fixed and imaged. Strikingly, while ERK7^{AID} parasites faithfully attached and invaded the cells, we observed a complete block in both attachment

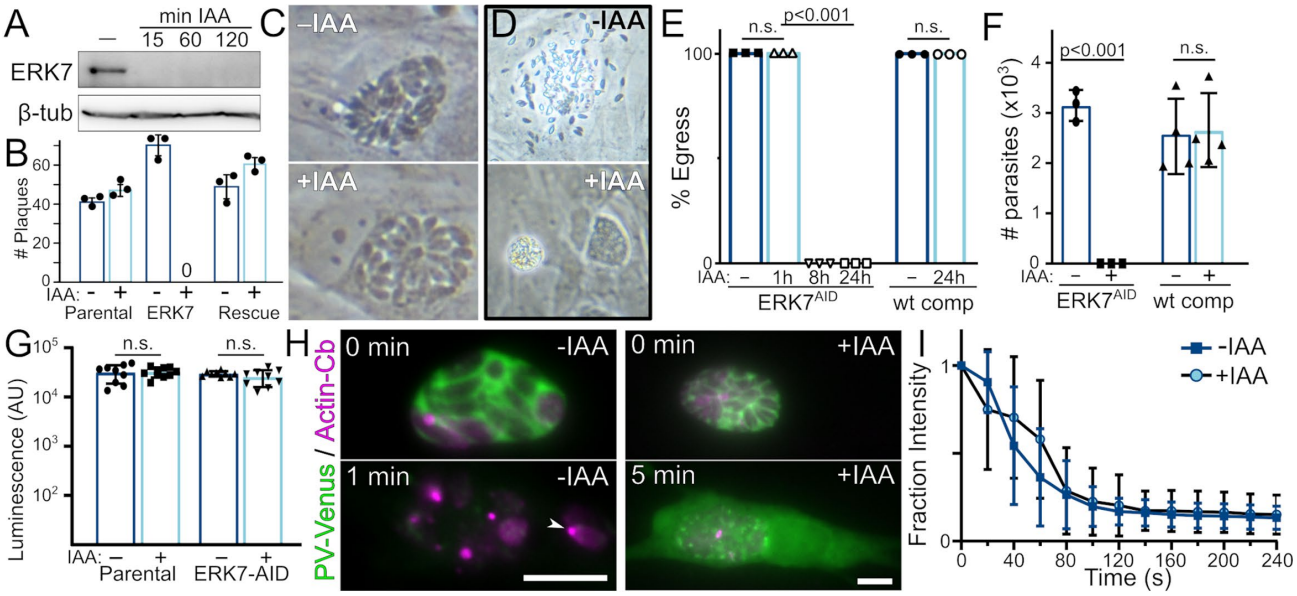

FIGURE 3: Loss of ERK7 blocks parasite invasion and egress. (A) ERK7^{AID} parasites were incubated as indicated with IAA and lysates were probed with anti-FLAG and anti–β-tubulin as a loading control. (B) Quantification of three replicate plaque assays with parental, ERK7^{AID}, and ERK7^{AID}(wt-comp) strains +/– IAA. (C) Phase image of ERK7^{AID} parasites grown 24 h +/– IAA. (D) Parasites as in C were grown 18 h more until vacuoles began to rupture. (E) Quantification of egress from $n = 3$ replicates grown as indicated in IAA. (F) Quantification of attached and invaded parasites from ERK7^{AID} and ERK7^{AID}(wt-comp) strains grown +/– IAA. (G) Quantification of *Gaussia* luciferase activity secreted by the indicated strains grown +/– IAA. (H) ERK7^{AID} and ERK7$^{AID/IAA}$ expressing an actin chromobody (magenta) and secreting Venus into the PV (green) were imaged at the indicated times after ionophore treatment. Scale bars: 10 µm. (I) Quantification of PV Venus signal of parasites as in H relative to the first frame ($n = 93$ –IAA; 81 +IAA). Error bars are SD.

and invasion in ERK7$^{AID/IAA}$ parasites, which was rescued when complemented with a wild-type copy (Figure 3F). These severe egress and invasion phenotypes fully explain the null plaque count we observed (Figure 3B).

ERK7 is required for parasite motility but not microneme secretion

Both egress and invasion require secretion of specialized organelles called the micronemes (Lourido *et al.*, 2012). ERK7 localizes to the apical end of the parasite (Figure 2), near the site from which the micronemes are thought to be secreted. Thus, ERK7 could act as a regulator of secretion. To test this hypothesis, we engineered the parental and ERK7^{AID} strains to express MIC2 fused to *Gaussia* luciferase (Brown *et al.*, 2016). Surprisingly, ERK7 depletion did not inhibit microneme secretion of this luciferase reporter (Figure 3G). The microneme protein PLP1 permeabilizes the parasitophorous vacuole (PV) to large macromolecules (Kafsack *et al.*, 2009). To confirm that ERK7 depletion did not block secretion of native microneme proteins, we used strains that secreted mVenus into the PV and measured mVenus diffusion from the PV after ionophore treatment to confirm PLP1 secretion (Figure 3H and Supplemental Movie 1). For the majority of vacuoles imaged (>90%), we observed permeabilization of the PV membrane within the 5 min of imaging after ionophore treatment, independent of growth in IAA and with similar dynamics (Figure 3I). However, while ERK7^{AID} parasites lysed out of the host cell shortly after permeabilization, ERK7$^{AID/IAA}$ parasites were immobile and trapped within their PV. For these ERK7$^{AID/IAA}$ vacuoles, mVenus signal remained within the host cell, which was not itself permeabilized. Taken together, these data indicate that functional microneme secretion occurs in the ERK7$^{AID/IAA}$ parasites, though they do not egress.

Toxoplasma parasites move using an unusual actin-based mechanism termed "gliding motility." Actin nucleation at the parasite's apical tip is essential to initiating this process (Tosetti *et al.*, 2019). We used an established actin "chromobody" (Periz *et al.*, 2017) to visualize F-actin dynamics during ionophore treatment. As expected, F-actin puncta quickly formed at the apical tips of the ERK7^{AID} parasites, preceding motility and the rapid egress described above (Figure 3H and Supplemental Movie 1). ERK7$^{AID/IAA}$ parasites, however, showed no change in their actin structures over 5 min of imaging (Figure 3H and Supplemental Movie 1). Thus, parasites that have developed without ERK7 cannot regulate their actin structures to initiate movement.

The parasite apical complex formation requires functional ERK7

The combination of phenotypes above and the requirement for a full cell cycle suggested that loss of ERK7 blocks the development of structures critical to parasite motility, invasion, and egress. Recently, the *Toxoplasma* conoid has been implicated in mediating these processes independently of any role in microneme secretion (Long *et al.*, 2017a,b; Nagayasu *et al.*, 2017; Tosetti *et al.*, 2019). We therefore examined transmission electron micrographs (TEM) of intracellular ERK7^{AID} parasites that had been grown with or without IAA for 18 h. Although we could easily identify the apical complex conoid with a "crown" of micronemes in ERK7^{AID} parasites (Figure 4A), we could find no evidence of a conoid in any ERK7$^{AID/IAA}$ parasites (Figure 4B).

The microtubule structures of the apical complex are preserved in detergent-extracted parasites. When we examined negatively stained detergent-extracted parasite "ghosts" by TEM (Figure 4, C–F), we found that ERK7 depletion results in a complete loss of the

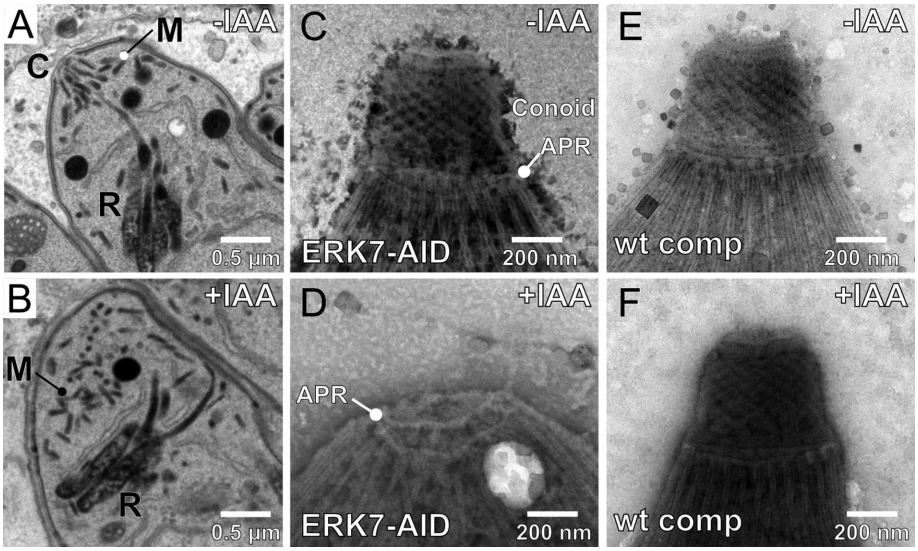

FIGURE 4: The apical complex is disrupted in parasites lacking ERK7. TEM of (A) ERK7^{AID} parasites develop normal conoids [C] and well organized secretory organelles (micronemes [M] and rhoptries [R]), while those grown (B) for 18 h in IAA have no identifiable conoid and disorganized secretory organelles. TEM of negatively stained detergent-extracted parasites reveal normal microtubule structures in ERK7^{AID} parasites ($n = 20$) (C) including the distinctive rings and conoid spiral of the apical complex, which are lost when parasites are grown for 18 h in IAA ($n = 60$; D). Complementation of ERK7^{AID} with wild-type ERK7 rescues all phenotypes ($n = 20$; E, F).

conoid structure, which is rescued by complementation with wild-type ERK7. This is striking for two reasons. First, the complete loss of the conoid is much more severe than previously reported phenotypes that caused only its deformation (Long *et al.*, 2017a; Nagayasu *et al.*, 2017). Second, previously reported phenotypes in the apical complex have been caused by disruption of proteins that localize to the complex itself, and therefore likely perform a structural role. ERK7, however, is not an apical complex protein, as it localizes just basal to the structure (Figure 2). These observations suggest ERK7 performs a regulatory role in conoid biogenesis. Notably, this profound ultrastructural defect appears to be specific to the conoid, as the 22 cortical microtubules appear unaffected by ERK7 degradation (Figure 4D). Consistent with this, the apical polar ring that is thought to form the microtubule-organizing center for the cortical microtubules (Leung *et al.*, 2017) appears to be preserved in parasites lacking ERK7.

In addition to the lack of conoids, we noted a striking disorganization of the micronemes and rhoptries in the TEMs of ERK7$^{AID/IAA}$ parasites (Figure 4B). To confirm these observations, we imaged parasites either expressing fluorescent-protein fusions or stained with available antibodies to a variety of markers (Figure 5). Consistent with our TEM data, the apical secretory organelles appeared disorganized when visualized by fluorescence microscopy. Staining with RON11 (which marks the apical rhoptry neck) and ROP2 (which marks the basal rhoptry bulb), we found that rhoptries do not bundle together upon ERK7 degradation and are not consistently oriented with their necks toward the parasite apical end (Figure 5A). These data suggest that loss of the conoid causes a failure in rhoptry tethering.

Fluorescence microscopy also showed that the microneme marker PLP1 was not aligned at the parasite plasma membrane in ERK7$^{AID/IAA}$ parasites. Instead, micronemes appear haphazardly arranged in the apical parasite cytosol (Figure 5B). Like other reports of conoid defects (Long *et al.*, 2017a; Nagayasu *et al.*, 2017), we observed functional microneme secretion upon ERK7 depletion and disruption of the apical complex (Figure 3). Our data indicate that micronemes must be secreted through a site distinct from the conoid in ERK7$^{AID/IAA}$ parasites.

We also examined markers for distinct substructures in the parasite's specialized cytoskeleton. The apical cap, as marked by ISP1, appeared to be preserved upon ERK7 degradation (Figure 5C). The apical polar ring marker RNG1-GFP also localized correctly in parasites lacking ERK7 (Figure 5D), consistent with the observed preservation of the cortical microtubules. These data confirm that ERK7 degradation leads to the specific disruption of the parasite conoid.

GFP-tubulin identifies the conoid as bright apical puncta, which was lost upon ERK7 degradation (Figure 5). These data demonstrate that the complete loss of conoid structure observed in the parasite ghosts was not an artifact of sample preparation. We used this phenotype to assess whether ERK7 kinase activity was required for its function in conoid biogenesis. Because we were unable to obtain parasites stably expressing kinase-dead ERK7, we used transient transfection. We transfected ERK7^{AID} parasites stably expressing GFP-tubulin with a plasmid encoding either wild-type or kinase-dead (D136A) HA-tagged ERK7 driven by its native promoter. ERK7^{AID} and ERK7$^{AID/IAA}$ parasites were fixed after 24-h growth, stained with anti-HA, and imaged. As expected, expression of wild-type ERK7 enabled ERK7$^{AID/IAA}$ parasites to form conoids (Supplemental Figure S2D). However, we did not observe rescue of conoid formation in ERK7$^{AID/IAA}$ parasites expressing kinase-dead ERK7 (Supplemental Figure S2D), indicating that kinase activity is required for ERK7 function in conoid biogenesis.

ERK7 is essential for conoid maturation

To understand the role of ERK7 in apical complex assembly, we tested whether ERK7 degradation altered the localization of other proteins that associate with the conoid. The *Toxoplasma* cartwheel protein orthologue SAS6L is normally associated with the conoidal rings (de Leon *et al.*, 2013). SAS6L colocalizes with GFP-tubulin foci in ERK7^{AID} parasites, and, like the conoid-localized tubulin, is lost in ERK7$^{AID/IAA}$ parasites (Figure 5E). Surprisingly, SAS6L and GFP-tubulin foci were found in the growing daughter buds of mature ERK7$^{AID/IAA}$ parasites that had lost their conoids.

Together, our data suggest that in parasites lacking ERK7, apical complex biogenesis initiates correctly but fails catastrophically during its maturation. To identify this point of failure, we infected a host monolayer with ERK7^{AID} parasites expressing GFP-tubulin, and incubated them in IAA for 8 h before fixation. As *Toxoplasma* replicates asynchronously, we could visualize multiple points in the cell cycle in a single experiment. As expected, all ERK7^{AID} parasites had clearly identifiable foci for GFP-tubulin and SAS6L at all points in the cell cycle (Figure 5F). Strikingly, we observed a loss of these foci only in ERK7$^{AID/IAA}$ parasites that had initiated or progressed through cytokinesis (Figure 5G). These conoid-deficient parasites then produced

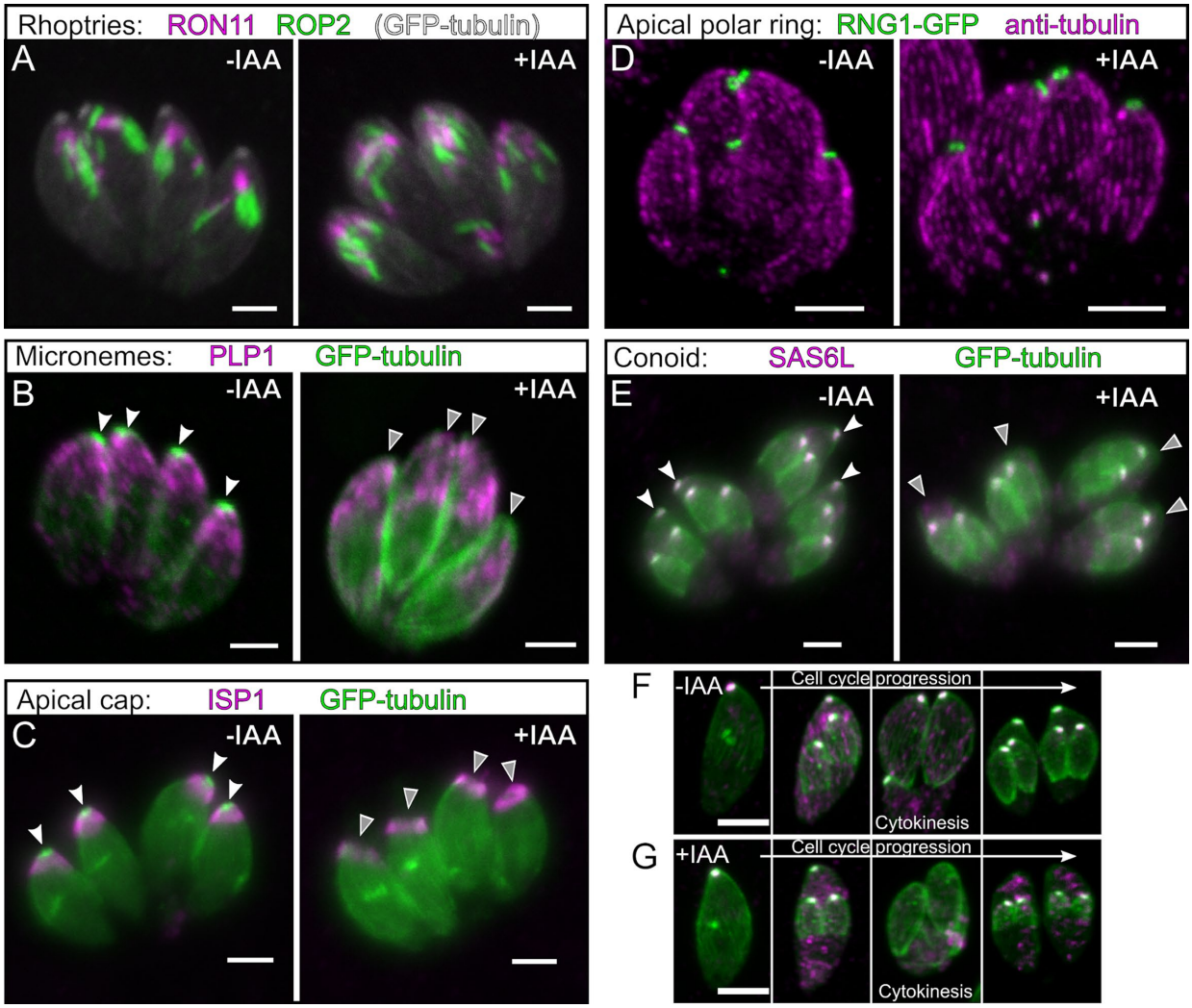

FIGURE 5: Loss of ERK7 results in disorganized apical structures. (A–E) ERK7^{AID} parasites were grown in +/− IAA and imaged using the indicated markers. All images are maximum intensity projections of confocal stacks. Scale bars: 3 μm. White arrows indicate the apical complex GFP-tubulin foci in mature parasites, which is missing in +IAA parasites (gray arrows). (F, G) ERK7^{AID} parasites were grown for 6 h in +/− IAA and imaged (GFP-tubulin, green; SAS6L, magenta). Scale bars: 4 μm.

daughters with clear tubulin/SAS6L apical foci. This indicates that without ERK7, the apical complex fails to insert correctly into the mother plasma membrane.

Conclusions

The cilia-like conoid is a key compartment for secretion and host invasion in *Toxoplasma*, but regulators of its function remain poorly characterized. Although ERK7 does not localize to the conoid, its loss of function results in the complete and specific disruption of the conoid structure. Our data indicate ERK7 is not a conoid structural protein, yet its loss causes a phenotype much more severe than the disruption of any known conoid-localized protein (Long *et al.*, 2017a,b; Nagayasu *et al.*, 2017). ERK7 orthologues are early-branching, but understudied, members of the MAPK protein kinase family (Supplemental Figure S1; Sang *et al.*, 2019), and our data suggest ERK7 is performing a regulatory role in *Toxoplasma* apical complex biogenesis. ERK7 orthologues in model organisms have implicated it in regulating diverse cellular processes, including autophagy (Colecchia *et al.*, 2012), protein trafficking and signaling (Zacharogianni *et al.*, 2011; Brzostowski *et al.*, 2013; Chia *et al.*, 2014; Bermingham *et al.*, 2017), and ciliogenesis (Miyatake *et al.*, 2015; Kazatskaya *et al.*, 2017). Given the diverse functions attributed to ERK7 in other phyla, it is likely *Toxoplasma* ERK7 plays nonessential roles in processes beyond conoid biogenesis.

Remarkably, ERK7 orthologues are found in all Eukaryotic kingdoms, but are expanded in ciliates (Supplemental Figure S1B; Eisen *et al.*, 2006) and strikingly missing in organisms that produce no cilia or flagella at any point in development, such as yeast and land plants. We have shown that ERK7 is essential for the biogenesis of a specialized cilium-like structure in *Toxoplasma gondii*, which suggests ERK7 has a conserved role as a critical regulator of ciliogenesis throughout Eukaryota. In metazoan cilia, ERK7 primarily localizes to the basal body (Figure 1A). Apicomplexans lack orthologues for many basal body proteins, and *Toxoplasma* has no identifiable basal body during its asexual stage (Francia *et al.*, 2015). We found ERK7 localized to the apical cytoskeletal cap that is delineated apically by the microtubule-organizing apical polar

ring and basally by the centrin-2–containing apical "annuli" (Engelberg *et al.*, 2019; Leung *et al.*, 2019). In a parallel study, we have demonstrated that disruption of an ERK7 scaffolding interaction blocks kinase recruitment to this site (Back *et al.*, 2020). In such parasites, ERK7 is restricted to the cytoplasm and the conoid does not form (Back *et al.*, 2020). We propose that *Toxoplasma* ERK7 functions at the apical cap to regulate the cytosol composition in the transition to the conoid, akin to ERK7 function at the metazoan cilia transition zone.

MATERIALS AND METHODS

Phylogenetic analysis

Protein sequences for human ERK1, JNK1, p38α, CDK1, ERK5, and ERK7/8, *Toxoplasma* ERK7 (TGME49_233010; ToxoDBv43, http://www.toxodb.org), and the ERK7 kinase domain sequences from the indicated organisms in Figure 1 were retrieved from Uniprot and aligned using Clustal Omega (Sievers *et al.*, 2011). The maximum likelihood phylogenetic tree and bootstrap analysis (1000 replicates) were estimated using RAxML v8.1.17 (Stamatakis, 2014).

PCR and plasmid generation

All PCR was conducted using Phusion polymerase (New England Biolabs) and primers listed in Supplemental Table 1. Constructs were assembled using Gibson master mix (New England Biolabs). Point mutations were created by the Phusion mutagenesis protocol.

Parasite culture and transfection

Human foreskin fibroblasts (HFF) were grown in DMEM supplemented with 10% fetal bovine serum and 2 mM glutamine. *Toxoplasma* tachyzoites were maintained in confluent monolayers of HFF. ERK7-3xHA and ERK7^{AID} strains were generated by transfecting the RHΔku80Δhxgprt strain (Huynh and Carruthers, 2009) or the same strain expressing OsTIR1 driven by the gra1-promoter with 50 µl of a PCR product using Q5 polymerase (New England Biolabs) with 500–base pair homology arms flanking a tag (3xHA or AID-3xFLAG) together with 5 µg of a Cas9 plasmid that had been modified to express HXGPRT and also a gRNA targeting the C-terminus of ERK7. The parasites were selected for HXGPRT expression for 2 d and immediately single cell cloned without selection. The ERK7^{AID} strain was complemented by targeting a 3xHA-tagged ERK7 driven by its native promoter, together with a bleomycin resistance cassette to the empty Ku80 locus, and selecting with bleomycin. GFP-α-tubulin, actin-chromobody, and SP-mVenus–expressing parasites were created by amplifying the FP-marker expression cassette and an adjacent chloramphenicol (or HXGPRT, in the case of SP-mVenus) resistance cassette by PCR and targeting it to a site adjacent Ku80 locus by CRISPR/Cas9-mediated homologous recombination (see Supplemental Table S1) and selecting with chloramphenicol (or MPA/Xan, as appropriate). The original pMIN eGFP-α-tubulin was a kind gift of Ke Hu (University of Indiana). The original pMIN actin chromobody-mEmerald was a kind gift of Aoife Heaslip (University of Connecticut). This vector was modified to replace the mEmerald with TdTomato. RNG1-eGFP, driven by its native promoter, was transiently transfected into parasites that were fixed after 18–24-h growth. Note that ERK7^{AID} parasites developed "escapees" after 1–2 mo of passage in which they ceased responding to IAA, and ERK7 was no longer degraded. All experiments were therefore conducted with parasites that had been cultured for <1 mo after cloning.

Plaque assays

To measure plaque efficiency, 200 of each parental, ERK7^{AID}, and ERK7^{AID}(wt-comp) parasites were allowed to infect confluent HFF in one well of a six-well plate in either the presence or absence of IAA. After 7 d, the monolayer was fixed with MeOH, stained with crystal violet, and the resulting plaques counted. All plaque assays were performed in biological triplicate.

Immunofluorescence

HFF cells were grown on coverslips in 24-well plates until confluent and were infected with parasites. The cells were rinsed twice with phosphate buffered saline (PBS), and were fixed with 4% paraformaldehyde (PFA)/4% sucrose in PBS at room temperature for 15 min. After two washes with PBS, cells were permeabilized with 0.1% Triton X-100 for 10 min and washed three times with PBS. After blocking in PBS + 3% bovine serum albumin for 30 min, cells were incubated in primary antibody in blocking solution overnight at room temperature. Cells were then washed three times with PBS and incubated with Alexa-Fluor conjugated secondary antibodies (Molecular Probes) for 2 h. Cells were then washed three times with PBS and then mounted with mounting medium containing DAPI (Vector Laboratories). For tyramide amplification of ERK7-AID-3xFLAG signal, the above protocol was altered as follows. Endogenous peroxidase activity was quenched by incubation of fixed coverslips with 100 mM sodium azide in PBS for 45 min at room temperature. Cells were blocked with 5% horse serum/0.5% Roche Western Blocking Reagent in TBST for 45 min. HRP-conjugated goat anti-mouse secondary antibody (Sigma) was used and tyramide-fluorophore was allowed to react for 30 s before final washes. Cells were imaged on either a Nikon A1 Laser Scanning Confocal Microscope, a Nikon Ti2E wide-field microscope, or a DeltaVision OMX SIM microscope. SIM stacks were deconvoluted and reconstructed using the manufacturer's recommended defaults. Primary antibodies used in this study include rat anti-HA 3F10 (Roche #11867423001), mouse m2 anti-FLAG (Sigma #F1804), rabbit anti–Tg-β-tubulin (1:10,000 dilution), rabbit anti-ROP2 (1:10,000 dilution), mouse-anti PLP1 (1:1000 dilution; gift of Vern Carruthers, University of Michigan), rat anti-RON11 (1:1000 dilution), mouse anti-ISP1 (1:1000 dilution), mouse anti-SAS6L (1:1000 dilution; final three antibodies were gifts of Peter Bradley, UCLA). Unless otherwise indicated, all micrographs are representative of 20 of 20 images collected. For SIM, images are representative of 5 of 5 stacks per staining condition.

Western blotting

Proteins were separated by SDS–PAGE and transferred to a polyvinylidene difluoride membrane. Membranes were blocked for 1 h in PBS + 5% milk, followed by overnight incubation at 4°C with primary antibody in blocking solution. The next day, membranes were washed three times with TBST, followed by incubation at room temperature for 1–2 h with HRP-conjugated secondary antibody (Sigma) in blocking buffer. After three washes with TBST, Western blots were imaged using ECL Plus reagent (Pierce) on a GE ImageQuant LAS4000. Antibodies used in this study include Rb anti–Tg-β-tubulin (1:1000 dilution), rat anti-HA (Sigma; 1:500 dilution), and mouse m2 anti-FLAG (Sigma; 1:1000 dilution).

Invasion and egress assays

For invasion assays, highly infected monolayers were mechanically disrupted by passage through a 27 gauge needle to release them. Parasites (3×10^6) of each strain tested (all expressing GFP-α-tubulin) were added to HFF monolayer grown in a 24-well plate with coverslip and incubated for 2 h at 37°C. These were then washed 10 times with PBS and fixed and prepared for imaging. A 3.15 mm^2 area (~1% of total well) was imaged per experiment and

images analyzed in ImageJ. For egress assays, parasites were allowed to grow for 24–30 h in HFF grown in a 24-well plate with coverslip. Parasites were washed with prewarmed hanks balanced salt solution (HBSS) before the assay, and then incubated with HBSS containing 1 µM calcium ionophore A23187 (Cayman Chemical) for 10 min at 37°C before fixation and imaging. Live-cell egress/PLP1-function assays were conducted as above, using cells plated in thin-bottom 96 wells for fluorescence microscopy (Corning) and imaged in a stage-top environment chamber (Tokai Hit) on a Nikon Ti2E microscope.

Transmission electron microscopy

Cells were fixed on MatTek dishes with 2.5% (vol/vol) glutaraldehyde in 0.1 M sodium cacodylate buffer. After three rinses in 0.1 M sodium cacodylate buffer, they were postfixed with 1% osmium tetroxide and 0.8% $K_3[Fe(CN_6)]$ in 0.1 M sodium cacodylate buffer for 1 h at room temperature. Cells were rinsed with water and en bloc stained with 2% aqueous uranyl acetate overnight. After three rinses with water, specimens were dehydrated with increasing concentration of ethanol, infiltrated with Embed-812 resin, and polymerized in a 70°C oven overnight. Blocks were sectioned with a diamond knife (Diatome) on a Leica Ultracut UC7 ultramicrotome (Leica Microsystems) and collected onto copper grids, poststained with 2% uranyl acetate in water and lead citrate. Parasite ghosts were prepared essentially as described in Nagayasu *et al.* (2017). Briefly, parasites were incubated with 20 µM calcium ionophore in HBSS at 37°C for 10 min. The parasite suspension was allowed to adhere to a grid, after which membranes were extracted by the addition of 0.5% Triton X-100 for 3–4 min. The samples were then stained with 2% phosphotungstic acid, pH 7.4. All TEM images were acquired on a Tecnai G2 spirit transmission electron microscope (FEI) equipped with a LaB_6 source at 120 kV. Images in Figure 4, A and B of sectioned cells are representative of 14 ERK^{AID} and 22 $ERK7^{AID/IAA}$ vacuoles imaged. Note that 86% of $ERK7^{AID}$ vacuoles imaged had at least one parasite with a visible conoid, while 0% of the $ERK7^{AID/IAA}$ vacuoles imaged had any observable conoid structure.

Figure generation

Data plotting and statistical analyses were conducted in Graphpad Prism v8.3. All error bars are SD and center values are means. Figure 3E was analyzed by one-way ANOVA with Tukey's test. All other *p* values are derived from two-tailed *t* test. All figures were created in Inkscape v0.92.

ACKNOWLEDGMENTS

We thank Josh Beck, Mike Henne, Vasant Muralidharan, and Ben Weaver for helpful comments on the manuscript; the UT Southwestern Electron Microscopy core facility for assistance with sample preparation; and Dorothy Mundy and the UT Southwestern Live Cell Imaging core facility for assistance with SIM image analysis. M.L.R. acknowledges funding from the Welch Foundation (I-1936-20170325) and National Science Foundation (MCB1553334). X.H. was funded, in part, by Cancer Prevention and Research Institute of Texas Training Grant no. RP160157. M.M. was funded, in part, by a National Science Foundation Graduate Research Fellowship (2019274212).

REFERENCES

Aikawa M (1967). Ultrastructure of the pellicular complex of *Plasmodium fallax*. J Cell Biol 35, 103–113.

Anderson-White B, Beck JR, Chen C-T, Meissner M, Bradley PJ, Gubbels M-J (2012). Cytoskeleton assembly in *Toxoplasma gondii* cell division. Int Rev Cell Mol Biol 298, 1–31.

Back PS, O'Shaughnessy WJ, Moon AS, Dewangan PS, Hu X, Sha J, Wohlschlegel JA, Bradley PJ, Reese ML (2020). Ancient MAPK ERK7 is regulated by an unusual inhibitory scaffold required for Toxoplasma apical complex biogenesis. BioRxiv 10.1101/2020.02.02.931089.

Bermingham DP, Hardaway JA, Refai O, Marks CR, Snider SL, Sturgeon SM, Spencer WC, Colbran RJ, Miller DM, Blakely RD (2017). The atypical MAP kinase SWIP-13/ERK8 regulates dopamine transporters through a Rho-dependent mechanism. J Neurosci 37, 9288–9304.

Brown KM, Lourido S, Sibley LD (2016). Serum albumin stimulates protein kinase G-dependent microneme secretion in *Toxoplasma gondii*. J Biol Chem 291, 9554–9565.

Brzostowski JA, Sawai S, Rozov O, Liao X-H, Imoto D, Parent CA, Kimmel AR (2013). Phosphorylation of chemoattractant receptors regulates chemotaxis, actin reorganization and signal relay. J Cell Sci 126, 4614–4626.

Carruthers VB, Sibley LD (1999). Mobilization of intracellular calcium stimulates microneme discharge in *Toxoplasma gondii*. Mol Microbiol 31, 421–428.

Chia J, Tham KM, Gill DJ, Bard-Chapeau EA, Bard FA (2014). ERK8 is a negative regulator of O-GalNAc glycosylation and cell migration. ELife 3, e01828.

Colecchia D, Strambi A, Sanzone S, Iavarone C, Rossi M, Dall'Armi C, Piccioni F, Verrotti di Pianella A, Chiariello M (2012). MAPK15/ERK8 stimulates autophagy by interacting with LC3 and GABARAP proteins. Autophagy 8, 1724–1740.

de Leon JC, Scheumann N, Beatty W, Beck JR, Tran JQ, Yau C, Bradley PJ, Gull K, Wickstead B, Morrissette NS (2013). A SAS-6-like protein suggests that the *Toxoplasma* conoid complex evolved from flagellar components. Eukaryot Cell 12, 1009–1019.

Eisen JA, Coyne RS, Wu M, Wu D, Thiagarajan M, Wortman JR, Badger JH, Ren Q, Amedeo P, Jones KM, *et al.* (2006). Macronuclear genome sequence of the ciliate *Tetrahymena thermophila*, a model eukaryote. PLoS Biol 4, e286.

Engelberg K, Chen C-T, Bechtel T, Sánchez Guzmán V, Drozda AA, Chavan S, Weerapana E, Gubbels M-J (2019). The apical annuli of *Toxoplasma gondii* are composed of coiled-coil and signalling proteins embedded in the inner membrane complex sutures. Cell Microbiol 22, e13112.

Francia ME, Dubremetz J-F, Morrissette NS (2015). Basal body structure and composition in the apicomplexans *Toxoplasma* and *Plasmodium*. Cilia 5, 3.

Francia ME, Jordan CN, Patel JD, Sheiner L, Demerly JL, Fellows JD, de Leon JC, Morrissette NS, Dubremetz J-F, Striepen B (2012). Cell division in Apicomplexan parasites is organized by a homolog of the striated rootlet fiber of algal flagella. PLoS Biol 10, e1001444.

Hepler PK, Huff CG, Sprinz H (1966). The fine structure of the exoerythrocytic stages of *Plasmodium fallax*. J Cell Biol 30, 333–358.

Hu K, Johnson J, Florens L, Fraunholz M, Suravajjala S, DiLullo C, Yates J, Roos DS, Murray JM (2006). Cytoskeletal components of an invasion machine—the apical complex of *Toxoplasma gondii*. PLoS Pathog 2, e13.

Huynh M, Carruthers VB (2009). Tagging of endogenous genes in a *Toxoplasma gondii* strain lacking Ku80. Eukaryot Cell 8, 530–539.

Kafsack BFC, Pena JDO, Coppens I, Ravindran S, Boothroyd JC, Carruthers VB (2009). Rapid membrane disruption by a perforin-like protein facilitates parasite exit from host cells. Science 323, 530–533.

Kazatskaya A, Kuhns S, Lambacher NJ, Kennedy JE, Brear AG, McManus GJ, Sengupta P, Blacque OE (2017). Primary cilium formation and ciliary protein trafficking is regulated by the atypical MAP kinase MAPK15 in *Caenorhabditis elegans* and human cells. Genetics 207, 1423–1440.

Lentini G, Dubois DJ, Maco B, Soldati-Favre D, Frénal K (2019). The roles of Centrin 2 and Dynein light chain 8a in apical secretory organelles discharge of *Toxoplasma gondii*. Traffic Cph Den 20, 583–600.

Leung JM, He Y, Zhang F, Hwang Y-C, Nagayasu E, Liu J, Murray JM, Hu K (2017). Stability and function of a putative microtubule-organizing center in the human parasite *Toxoplasma gondii*. Mol Biol Cell 28, 1361–1378.

Leung JM, Liu J, Wetzel LA, Hu K (2019). Centrin2 from the human parasite *Toxoplasma gondii* is required for its invasion and intracellular replication. J Cell Sci 132, jcs228791.

Lévêque MF, Berry L, Besteiro S (2016). An evolutionarily conserved SSNA1/DIP13 homologue is a component of both basal and apical complexes of *Toxoplasma gondii*. Sci Rep 6, 27809.

Li Z-Y, Wang Z-D, Huang S-Y, Zhu X-Q, Liu Q (2016). TgERK7 is involved in the intracellular proliferation of *Toxoplasma gondii*. Parasitol Res 115, 34193424.

Long S, Anthony B, Drewry LL, Sibley LD (2017a). A conserved ankyrin repeat-containing protein regulates conoid stability, motility and cell invasion in *Toxoplasma gondii*. Nat Commun 8, 2236.

Long S, Brown KM, Drewry LL, Anthony B, Phan IQH, Sibley LD (2017b). Calmodulin-like proteins localized to the conoid regulate motility and cell invasion by *Toxoplasma gondii*. PLoS Pathog 13, e1006379.
Lourido S, Tang K, Sibley LD (2012). Distinct signalling pathways control *Toxoplasma* egress and host-cell invasion. EMBO J 31, 4524–4534.
Lumb R, Smith K, O'Donoghue PJ, Lanser JA (1988). Ultrastructure of the attachment of *Cryptosporidium* sporozoites to tissue culture cells. Parasitol Res 74, 531–536.
Miyatake K, Kusakabe M, Takahashi C, Nishida E (2015). ERK7 regulates ciliogenesis by phosphorylating the actin regulator CapZIP in cooperation with Dishevelled. Nat Commun 6, 6666.
Nagayasu E, Hwang Y-C, Liu J, Murray JM, Hu K (2017). Loss of a double-cortin (DCX)-domain protein causes structural defects in a tubulin-based organelle of *Toxoplasma gondii* and impairs host-cell invasion. Mol Biol Cell 28, 411–428.
Nishi M, Hu K, Murray JM, Roos DS (2008). Organellar dynamics during the cell cycle of *Toxoplasma gondii*. J Cell Sci 121, 1559–1568.
Nishimura K, Fukagawa T, Takisawa H, Kakimoto T, Kanemaki M (2009). An auxin-based degron system for the rapid depletion of proteins in nonplant cells. Nat Methods 6, 917–922.
Okamoto N, Keeling PJ (2014). The 3D structure of the apical complex and association with the flagellar apparatus revealed by serial TEM tomography in *Psammosa pacifica*, a distant relative of the Apicomplexa. PLoS One 9, e84653.
Periz J, Whitelaw J, Harding C, Gras S, Del Rosario Minina MI, Latorre-Barragan F, Lemgruber L, Reimer MA, Insall R, Heaslip A, *et al*. (2017). *Toxoplasma gondii* F-actin forms an extensive filamentous network required for material exchange and parasite maturation. ELife 6, e24119.
Portman N, Foster C, Walker G, Šlapeta J (2014). Evidence of intraflagellar transport and apical complex formation in a free-living relative of the apicomplexa. Eukaryot Cell 13, 10–20.
Sang D, Pinglay S, Wiewiora RP, Selvan ME, Lou HJ, Chodera JD, Turk BE, GümüşZH, Holt LJ (2019). Ancestral reconstruction reveals mechanisms of ERK regulatory evolution. ELife 8, e38805.
Sievers F, Wilm A, Dineen D, Gibson TJ, Karplus K, Li W, Lopez R, McWilliam H, Remmert M, Söding J, *et al*. (2011). Fast, scalable generation of high-quality protein multiple sequence alignments using Clustal Omega. Mol Syst Biol 7, 539.
Stamatakis A (2014). RAxML version 8: a tool for phylogenetic analysis and post-analysis of large phylogenies. Bioinforma Oxf Engl 30, 1312–1313.
Tosetti N, Dos Santos Pacheco N, Soldati-Favre D, Jacot D (2019). Three F-actin assembly centers regulate organelle inheritance, cell-cell communication and motility in *Toxoplasma gondii*. ELife 8, e42669.
Zacharogianni M, Kondylis V, Tang Y, Farhan H, Xanthakis D, Fuchs F, Boutros M, Rabouille C (2011). ERK7 is a negative regulator of protein secretion in response to amino-acid starvation by modulating Sec16 membrane association. EMBO J 30, 3684–3700.